Multiparticle Cumulant Mapping for Coulomb Explosion Imaging

Chuan Cheng, Leszek J. Frasinski, Gönenç Moğol, Felix Allum, Andrew J. Howard, Daniel Rolles, Philip H. Bucksbaum, Mark Brouard, Ruaridh Forbes, and Thomas Weinacht

Phys. Rev. Lett. **130**, 093001 — Published 2 March 2023

DOI: 10.1103/PhysRevLett.130.093001

Multi-Particle Cumulant Mapping for Coulomb Explosion Imaging

Chuan Cheng,[1] Leszek J. Frasinski,[2] Gönenç Moğol,[1] Felix Allum,[3,4,5] Andrew J. Howard,[4,6] Daniel Rolles,[7] Philip H. Bucksbaum,[4,5] Mark Brouard,[3] Ruaridh Forbes,[4,5] and Thomas Weinacht[1]

[1]*Department of Physics and Astronomy, Stony Brook University, Stony Brook, New York 11794, USA*
[2]*Department of Physics, Imperial College London, Prince Consort Road, London SW7 2AZ, United Kingdom*
[3]*Chemistry Research Laboratory, Department of Chemistry, University of Oxford, Oxford OX1 3TA, United Kingdom*
[4]*Stanford PULSE Institute, SLAC National Accelerator Laboratory, Menlo Park, California 94025, USA*
[5]*Linac Coherent Light Source, SLAC National Accelerator Laboratory, Menlo Park, California 94025, USA*
[6]*Department of Applied Physics, Stanford University, Stanford, California 94305, USA*
[7]*J. R. Macdonald Laboratory, Department of Physics, Kansas State University, Manhattan, Kansas 66506, USA*

We extend covariance velocity map ion imaging to four particles, establishing cumulant mapping and allowing for measurements that provide insights usually associated with coincidence detection, but at much higher count rates. Without correction, a four-fold covariance analysis is contaminated by the pairwise correlations of uncorrelated events, but we have addressed this with the calculation of a full cumulant, which subtracts pairwise correlations. We demonstrate the approach on the four-body breakup of formaldehyde following strong field multiple ionization in few-cycle laser pulses. We compare Coulomb explosion imaging for two different pulse durations (30 fs and 6 fs), highlighting the dynamics that can take place on ultrafast timescales. These results have important implications for Coulomb explosion imaging as a tool for studying ultrafast structural changes in molecules, a capability that is especially desirable for high-count rate x-ray free electron laser experiments.

Multi-particle coincidence measurements have provided a remarkable window into the structure and dynamics of small molecules [1–10]. In particular, Coulomb explosion imaging (CEI) can provide insight into many structural changes occurring in photoexcited molecules including isomerization [11–13], dissociation [14–21], roaming [22–25] , Hydrogen migration [26, 27] and bond-cleavage [28]. CEI relies on multiple ionization of the target molecule, followed by a measurement of the relative momenta of the resultant ionic fragments, from which structural information can be inferred. Particularly for larger molecules, a high degree of ionization and fragmentation of the target must be achieved and many fragments must be detected in order to extract meaningful structural information. This technique is of great interest because it can provide time resolved information on molecular structure in the recoil frame. Recently, both strong field ionization and X-ray multiphoton ionization induced CEI have yielded promising results in studies that make use of multi-particle correlations [12, 19, 22, 29–31].

While coincidence measurements have been extremely useful for establishing multi-particle correlations, the low event rates required to avoid false coincidences make the repeated measurements necessary for tracking time dependent structural changes challenging [7]. Fortunately, in the high event rate regime, covariance analysis that measures linear correlation among particles has been developed and widely used for two-body and three-body correlations [32–34]. Some tabletop and free-electron laser (FEL) based experiments have already incorporated this statistical analysis technique [7, 16, 19, 34–37]. While experiments at FEL beamlines have drawn a lot of attention, FEL pulses are subject to large temporal and spectral fluctuations. These can be dealt with using more extended techniques, such as partial and contingent covariance [38–40]. However, covariance measurements have not yet been established in four-or-more body relationships because four-body and higher covariance is qualitatively different from two- and three-body [39, 41]. This can be seen by evaluating the expressions for collective correlations amongst a few fragments:

$$\chi_n(A,B,...) = \langle (N_A - \langle N_A \rangle)(N_B - \langle N_B \rangle)(...) \rangle, \quad (1)$$

where χ_n is the n-fold covariance and N_A denotes the number of fragments of species A generated in a given measurement. The brackets $\langle ... \rangle$ represent an expectation value. If one assumes tha the number of fragments follows a Poisson distribution, then one can show that [41][42]:

$$\begin{aligned} \chi_2(A,B) &= \langle N_{AB} \rangle, \\ \chi_3(A,B,C) &= \langle N_{ABC} \rangle, \\ \chi_4(A,B,C,D) &= \langle N_{ABCD} \rangle + \sum^{3} \langle N_{AB} \rangle \langle N_{CD} \rangle. \end{aligned} \quad (2)$$

Here the sum is over the three ways of pairing the four variables. N_{AB} (similar for N_{ABC}, etc.) denotes the number of events in which fragments A and B are generated together (e.g. $CD_2O^{2+} \longrightarrow CD_2^+ + O^+$).

Starting from the 4^{th} order covariance, χ_n will have contributions from pairwise correlations $\langle N_{AB} \rangle \langle ... \rangle$ that are independent or separate from the full N body correlations of interest. This will lead to a non-zero correlation value even in the absence of collective correlation amongst all N fragments [39]. With a small correction, the covariance formula can be modified to capture only

the full four-body correlations, which is equivalent to a four-fold cumulant [41]:

$$\varkappa_4 = \chi_4 - \sum^{3} \chi_2(A,B)\chi_2(C,D) = \langle N_{ABCD} \rangle. \quad (3)$$

In this manuscript, we focus on demonstrating the power of the new four-fold cumulant mapping, $\varkappa_4$, by investigating the fragmentation of strong field ionized formaldehyde (undeuterated and deuterated). First we show that this method can determine the relative, correlated momenta of all the ionic fragments produced by full Coulomb explosion of the molecule into atomic constituents. This is achieved at relatively high count rates and short data acquisition times, essential for the extension of this technique to time-resolved measurements. Then we show that a four-fold covariance analysis of the data is contaminated by the effect of pairwise correlations between the ions, which is eliminated by using the full cumulant formula. Finally, we use the method to contrast the Coulomb explosion dynamics of formaldehyde with 30 fs and 6 fs pulses. This shows that the fragmentation dynamics are more complex for the 30 fs case, in contrast to the 6 fs case, where the dynamics more closely match the expectation for a swift Coulomb repulsion following impulsive ionization of the molecule.

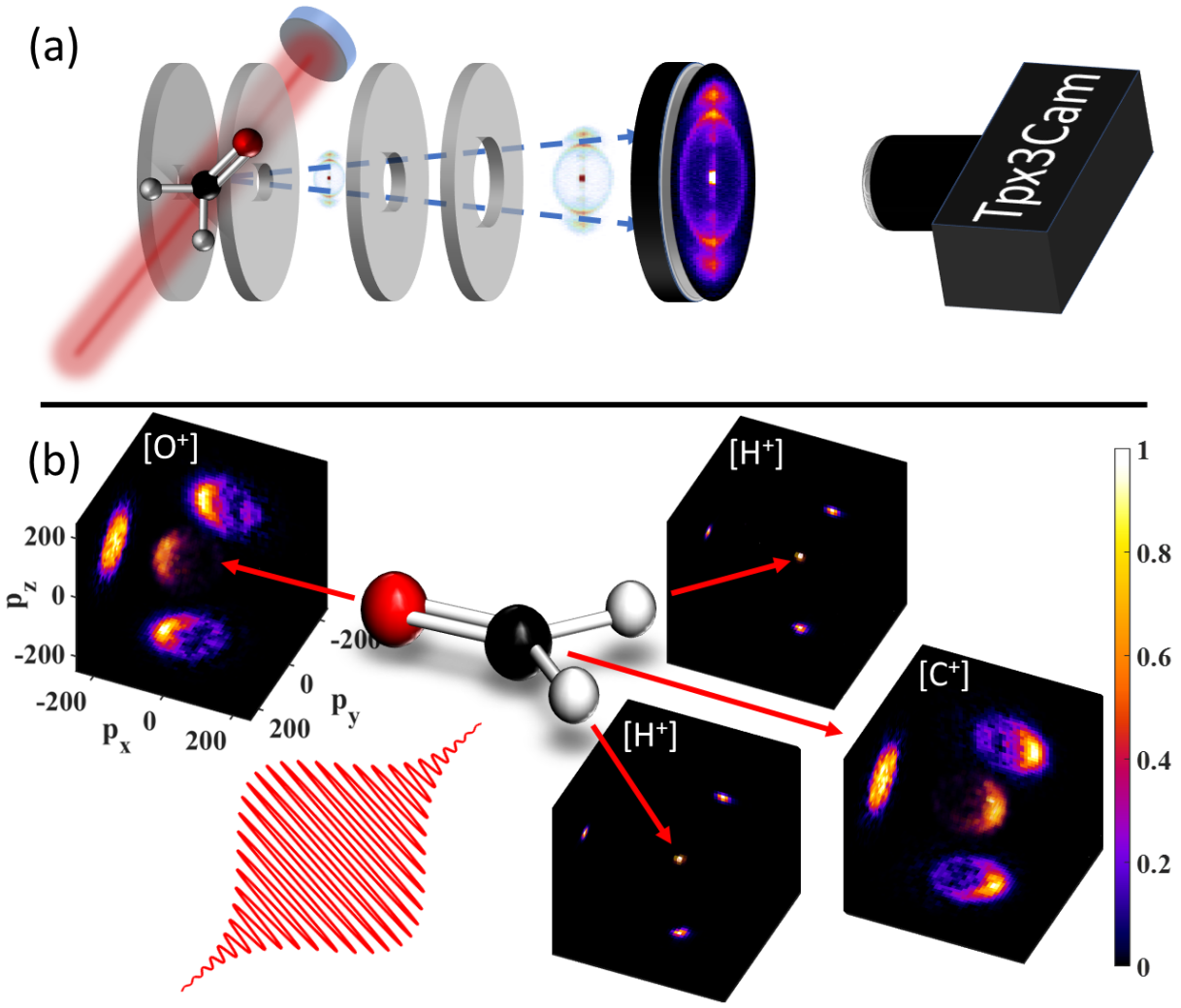

FIG. 1. Diagram of the experimental setup and demonstration of recoil frame reconstruction using the four-fold cumulant: $\varkappa_4$(H^+,H^+,C^+,O^+). Panel (a) shows the VMI assembly, where ionization happens and fragments are accelerated toward microchannel plates (MCP) and phosphor. The phosphor is imaged on the Tpx3Cam camera and centroided to obtain 3D ion momentum. Panel (b) shows four-fold momentum resolved covariance of fragments from the quadruple ionization of CH_2O using a 30 fs, 800 nm, 240 TW/cm^2 linearly polarized pulse. The positive x-axis and xy-plane are defined by the momenta of the two protons, with the positive x-axis defined by their bisector. Momentum units are $\hbar/a_0$. A ball and stick model of the molecule is included to illustrate the relationship between the correlated momenta and the recoil frame.

Our experiments make use of a velocity map imaging (VMI) apparatus [43] outfitted with a Tpx3Cam cam-

era [44], illustrated in Figure 1 (a). The laser pulses originate from a commercial amplified Ti:sapphire laser system, which produces 30 fs laser pulses with 1 mJ of energy at a repetition rate of 1 kHz. The pulses are spectrally broadened in a stretched hollow core fiber (S-HCF) [45–48], and compressed using chirped mirrors to a minimum duration of about 6 fs. The pulses (30 fs from the amplifier or 6 fs from the S-HCF) are focused into our VMI apparatus.

The sample, deuterated or undeuterated formaldehyde, is obtained by sublimation of paraformaldehyde (purity 98%, Sigma–Aldrich) at 50–60°C. A skimmed molecular beam of sample molecules intersects the laser in the VMI apparatus.

The ionized fragments are accelerated toward the microchannel plates (MCP) and phosphor screen under velocity-mapping condition. The fluorescence from hits on the phosphor screen is imaged onto the camera with an $f/0.95$ lens. The 1 ns precision of the Tpx3Cam is sufficient to resolve the ion's momentum along the time-of-flight (ToF) direction, which can be used to reconstruct the full 3D-vector momenta of ions [7, 44, 49]. For the data presented here, the typical acquisition time was approximately 20 minutes, with on average 8 ions detected per shot. The detection efficiency of our apparatus is estimated to be $\eta = 60\%$ to 90% per particle resulting in a four-fold channel overall efficiency of around $\eta^4 = 13\%$ to 65% [41].

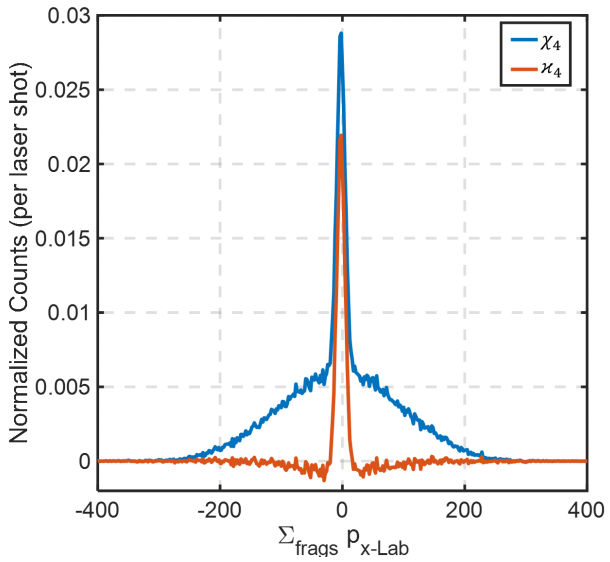

FIG. 2. Demonstration of momentum conservation along the lab frame laser polarization direction (x) for four-body dissociation of quadruply ionized deuterated formaldehyde (D^+, D^+, C^+, O^+) using 30 fs 240 TW/cm^2 laser pulses. Momentum units are $\hbar/a_0$. The blue curve shows a histogram using χ_4, and the red curve represents $\varkappa_4$ (see Eq. 2 and 3).

The full 3D information of correlated particles can be used to reconstruct the recoil frame and determine the kinetic energy release and angular distributions in the same way as coincidence measurements [7, 37]. A description of the algorithm to compute the four-body cumulants is provided in the Supplementary Information. In our approach, the computational complexity has been simplified by introducing approximations such that we are able to compute them in reasonable amount of time (≈ 1 min). The detailed discussion on this technical point is discussed in a separate publication.

The recoil frame can be defined in the following way: the bisector of two $H^+(D^+)$ unit momentum vectors defines the positive x-axis, while the difference between the two H^+ momenta unit vectors defines the positive y-axis. The positive z-axis can then be defined by computing the vector cross product of x and y. The definition is illustrated in Supplementary Figure S1. Once the recoil frame is defined for each H^+ pair, one can project the momenta of all four particles onto that frame. Figure 1 (b) shows the correlated momentum distribution of all four particles in this frame. As can be seen from panel (b), the O^+ is ejected preferentially along the negative x-axis, which is opposite to the two H^+, while the C^+ momentum is mostly along the positive x direction. Such a distribution bears a clear resemblance to the initial molecular geometry. A ball-and-stick model of the molecule is included in the figure to illustrate the fragmentation.

As a further test of the four-fold cumulant mapping method, we consider momentum conservation for four fragment ions. Figure 2 shows the comparison of the momentum sum along the lab frame x direction (laser polarization direction) of the four fragments using χ_4 or $\varkappa_4$. Here, a deuterated sample was used to avoid counting H^+ produced by background gases in the chamber. Due to momentum conservation in a full four-body breakup of the tetracation, we can see a sharp peak located at zero in both cases. The width of the distribution essentially reflects the momentum resolution of our detection apparatus.

For the curve depicting χ_4, in addition to the narrow peak at zero, we see that there is a broad peak extending over 200 $\hbar/a_0$. It arises from the product of two particle correlation terms: $\Sigma\chi_2(N_1, N_2)\chi_2(N_3, N_4)$. All fragment ion pairs contribute to this term, resulting in a roughly Gaussian distributed background. This illustrates the importance of using the correction in calculating the appropriate four particle correlation, which is equivalent to the calculation of a cumulant [41].

In contrast, the corrected correlation calculation, $\varkappa_4$, yields an almost perfect delta function, despite some small negative values between $\pm 100\ \hbar/a_0$, which can arise from small fluctuations in the molecular density or laser intensity [34, 39, 50, 51], or overlapping hits on the detector. Various techniques have been proposed to solve the fluctuation issue [38–40]. Further investigation is required in the context of a four-fold analysis. Note that the momentum conservation that we obtained here is not assumed or enforced by the algorithm, meaning that it comes out directly from the cumulant calculation. This

is a strong indication that our approach isolates signals from the four-body fragmentation of interest. Further evidence can be found in the progression of correlation orders in the conventional ToF-ToF analysis, which is provided in the Supplementary Information.

In order to highlight the ability of four particle correlations to capture pulse shape or time-dependent structural changes, we compare the O^+ distribution from covariant four particle measurements (such as the one shown in Figure 1) for 30 fs and 6 fs pulses. These results are shown in Figure 3. Compared to the O^+ from a 30 fs pulse, the yield from a 6 fs pulse has a significantly lower signal-to-noise ratio due to fewer counts, and it is more centered on the x-axis. This observation is consistent with earlier coincidence measurements on the same molecule using 7 fs pulses [52]. The significantly higher yield and broader angle distribution for the 30 fs pulse as compared to the 6 fs pulse can be related to dynamics during the ionization processes. Enhanced ionization has been observed to increase the production of high charge states in many small molecules, facilitated by dynamics on lower charge states during the pulse. [31, 53–58].

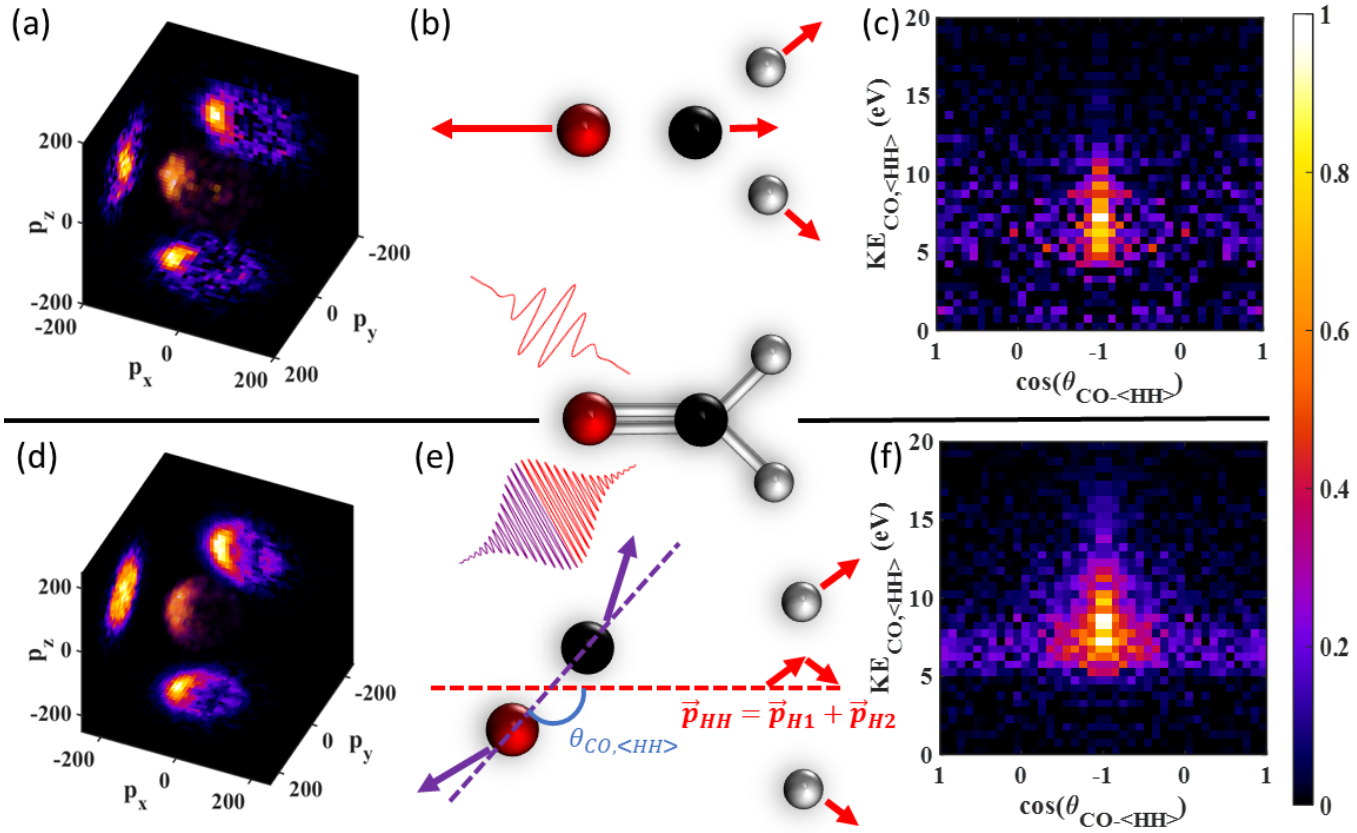

FIG. 3. Comparison of CEI with 6 fs 1300 TW/cm^2 pulses (top row) and 30 fs 240 TW/cm^2 pulses (bottom row) using four-fold cumulant imaging $\varkappa_4(H^+,H^+,C^+,O^+)$. Panels (a) and (d) show 3D histograms of the O^+ momentum distribution in the recoil frame, similar to Figure 1. Momentum units are $\hbar/a_0$. Panels (b) and (e) depict possible concerted and sequential breakup dynamics of the molecule for short (6 fs) or long (30 fs) pulses, respectively. The laser pulse and momentum vectors of the four fragments are also colored to indicate a possible time ordering of the breakup process. Panels (c) and (f) show a native frames analysis of panels (a) and (d) by correlating the dissociation energy of the CO^{2+} fragment and the native frame angle (CO/<HH>), assuming the two H^+ ions leave first. The angle axis is mirrored to put the main distribution in the center.

Dynamics during ionization (e.g. rotation of the CO fragment after C–H dissociation) for the 30 fs pulses can also lead to broader angular distributions of the O^+ fragment, as illustrated in Figure 3. It is not clear from our measurements if the C–O dissociation takes place during the laser pulse, but it is clear that some rotation takes place after H^+ dissociation, but before dissociation is complete. Similar dynamics are considered in the coincidence imaging of the 3-body channels (H^+,H^+,CO^+) and (H^+,CH^+,O^+) studied in earlier work [52].

Our single pulse measurements cannot rule out other possibilities, such as sequential dissociation of (<HH>, CO) with subsequent rotation and dissociation of the CO. It has been demonstrated recently that a native frame analysis, making use of three body Jacobi coordinates, can be very useful in separating sequential from concerted dynamics [40, 59, 60]. Briefly, in sequential dissociation, there is competition between rotation and the second dissociation, resulting in a broad angular distribution for the fragments resulting from the second dissociation. The

analysis is usually carried out for three-body problems, whereas there are four fragments in the present dissociation channel. Thus, we consider the dissociation of the two H^+ as a single initial event, with their center of mass momentum represented by <HH>, with the OC^{2+} breakup being a separate event, which can happen concertedly or sequentially, after the C–H dissociation. The native frame angles between CO^{2+} and <HH>, as well as the dissociation energy of (C^+, O^+) are shown in Figure 3 panel (e). In this frame, it is clear that between a dissociation energy of 5–8 eV, the 30 fs pulse data has a long tail outside the main peak at 180°, while 6 fs does not. A clear difference in the ionization dynamics for the two pulse durations is spotted, which suggests that the C–O dissociation takes place sequentially, after the C–H dissociation. The kinetic energy released into the (C^+, O^+) pair is in good agreement with the CO^{2+} dissociation energy measured in earlier coincidence experiments with OCS [59], suggesting that the same metastable CO^{2+} intermediate is involved. A time-dependent (i.e. pump-probe) measurement would be required to reveal the full dissociation dynamics, for which high count rate covariance measurements are key.

In conclusion, we have demonstrated the experimental implementation of four-particle cumulant velocity map imaging, which can be used to track ultrafast structural dynamics in small molecules. We illustrate the importance of using the four-fold cumulant $\varkappa_4$ over four-fold covariance χ_4 by confirming momentum conservation in channel (D^+, D^+, C^+, O^+). Our analysis highlights the ability to view the explosion dynamics in the recoil frame, and demonstrates the sensitivity to ultrafast dynamics using high-fold cumulants. While the single pulse measurements presented here do not provide a full picture of the dynamics in question, they motivate and enable time-resolved pump-probe measurements with cumulant analysis, which can be carried out with count rates about two orders of magnitude higher than coincidence measurements. We anticipate that cumulant mapping will be particularly valuable for analysing the Coulomb explosion induced by XFELs, where the X-ray intensity is so high that coincidence analysis becomes overwhelmed by the event rate. Moreover, this analysis is not restricted to four-fold. Cumulants with even higher order are now accessible using the proposed algorithm.

Acknowledgments

F.A. acknowledges the EPSRC for their support. M.B. gratefully acknowledges support of the EPSRC (Programme Grant No. EP/V026690/1). R.F. acknowledges support from the Linac Coherent Light Source, SLAC National Accelerator Laboratory, which is supported by the US Department of Energy, Office of Science, Office of Basic Energy Sciences, under contract no. DE-AC02-76SF00515. In addition, R.F., F.A., and P.H.B. were supported by the U.S. Department of Energy, Office of Science, Basic Energy Sciences, Chemical Sciences, Geosciences, and Biosciences Division, AMOS Program under SLAC FWP SCW0063. D.R. was supported by contract no. DE-FG02-86ER13491 from the same agency. A.J.H. was supported by the National Science Foundation. A.J.H. was additionally supported under a Stanford Graduate Fellowship as the 2019 Albion Walter Hewlett Fellow. C.C., G.M. and T.W. acknowledge support from the US Department of Energy under Award No. DEFG02-08ER15984. The authors thank Taran Driver (SLAC National Accelerator Laboratory) for fruitful discussions and for helping to facilitate this research collaboration.

[1] J. Eland, Dynamics of fragmentation reactions from peak shapes in multiparticle coincidence experiments, Laser Chemistry **11**, 259 (1991).

[2] M. Lavollée and H. Bergeron, Data treatment in multiparticle coincidence experiments: two-step dissociation processes, Journal of Physics B: Atomic, Molecular and Optical Physics **25**, 3101 (1992).

[3] A. Landers, T. Weber, I. Ali, A. Cassimi, M. Hattass, O. Jagutzki, A. Nauert, T. Osipov, A. Staudte, M. Prior, et al., Photoelectron diffraction mapping: Molecules illuminated from within, Physical Review Letters **87**, 013002 (2001).

[4] L. Holmegaard, J. L. Hansen, L. Kalhøj, S. Louise Kragh, H. Stapelfeldt, F. Filsinger, J. Küpper, G. Meijer, D. Dimitrovski, M. Abu-Samha, et al., Photoelectron angular distributions from strong-field ionization of oriented molecules, Nature Physics **6**, 428 (2010).

[5] T. Jahnke, T. Weber, T. Osipov, A. Landers, O. Jagutzki, L. P. H. Schmidt, C. Cocke, M. Prior, H. Schmidt-Böcking, and R. Dörner, Multicoincidence studies of photo and Auger electrons from fixed-in-space molecules using the COLTRIMS technique, Journal of Electron Spectroscopy and Related Phenomena **141**, 229 (2004).

[6] A. Staudte, S. Patchkovskii, D. Pavičić, H. Akagi, O. Smirnova, D. Zeidler, M. Meckel, D. Villeneuve, R. Dörner, M. Y. Ivanov, et al., Angular tunneling ionization probability of fixed-in-space h 2 molecules in intense laser pulses, Physical Review Letters **102**, 033004 (2009).

[7] F. Allum, C. Cheng, A. J. Howard, P. H. Bucksbaum, M. Brouard, T. Weinacht, and R. Forbes, Multi-particle three-dimensional covariance imaging:"coincidence" insights into the many-body fragmentation of strong-field ionized D2O, The Journal of Physical Chemistry Letters **12**, 8302 (2021).

[8] F. Légaré, K. F. Lee, I. Litvinyuk, P. Dooley, S. Wesolowski, P. Bunker, P. Dombi, F. Krausz, A. Bandrauk, D. Villeneuve, et al., Laser Coulomb-explosion imaging of small molecules, Physical Review A **71**, 013415 (2005).

[9] M. Pitzer, M. Kunitski, A. S. Johnson, T. Jahnke, H. Sann, F. Sturm, L. P. H. Schmidt, H. Schmidt-

Böcking, R. Dörner, J. Stohner, et al., Direct determination of absolute molecular stereochemistry in gas phase by Coulomb explosion imaging, Science **341**, 1096 (2013).
[10] K. Fehre, S. Eckart, M. Kunitski, M. Pitzer, S. Zeller, C. Janke, D. Trabert, J. Rist, M. Weller, A. Hartung, et al., Enantioselective fragmentation of an achiral molecule in a strong laser field, Science Advances **5**, eaau7923 (2019).
[11] Y. Jiang, A. Rudenko, O. Herrwerth, L. Foucar, M. Kurka, K. Kühnel, M. Lezius, M. F. Kling, J. van Tilborg, A. Belkacem, et al., Ultrafast extreme ultraviolet induced isomerization of acetylene cations, Physical Review Letters **105**, 263002 (2010).
[12] S. Bhattacharyya, K. Borne, F. Ziaee, S. Pathak, E. Wang, A. S. Venkatachalam, X. Li, N. Marshall, K. D. Carnes, C. W. Fehrenbach, et al., Strong-field-induced Coulomb explosion imaging of tribromomethane, The Journal of Physical Chemistry Letters **13**, 5845 (2022).
[13] M. Burt, K. Amini, J. W. Lee, L. Christiansen, R. R. Johansen, Y. Kobayashi, J. D. Pickering, C. Vallance, M. Brouard, and H. Stapelfeldt, Communication: Gas-phase structural isomer identification by Coulomb explosion of aligned molecules, The Journal of Chemical Physics **148**, 091102 (2018).
[14] I. Bocharova, A. Alnaser, U. Thumm, T. Niederhausen, D. Ray, C. L. Cocke, and I. Litvinyuk, Time-resolved Coulomb-explosion imaging of nuclear wave-packet dynamics induced in diatomic molecules by intense few-cycle laser pulses, Physical Review A **83**, 013417 (2011).
[15] S. De, M. Magrakvelidze, I. Bocharova, D. Ray, W. Cao, I. Znakovskaya, H. Li, Z. Wang, G. Laurent, U. Thumm, et al., Following dynamic nuclear wave packets in N_2, O_2, and CO with few-cycle infrared pulses, Physical Review A **84**, 043410 (2011).
[16] F. Allum, M. Burt, K. Amini, R. Boll, H. Köckert, P. K. Olshin, S. Bari, C. Bomme, F. Brauße, B. Cunha de Miranda, et al., Coulomb explosion imaging of CH_3I and CH_2ClI photodissociation dynamics, The Journal of Chemical Physics **149**, 204313 (2018).
[17] M. Burt, R. Boll, J. W. Lee, K. Amini, H. Köckert, C. Vallance, A. S. Gentleman, S. R. Mackenzie, S. Bari, C. Bomme, et al., Coulomb-explosion imaging of concurrent CH_2BrI photodissociation dynamics, Physical Review A **96**, 043415 (2017).
[18] X. Ding, R. Forbes, M. Kübel, K. F. Lee, M. Spanner, A. Y. Naumov, D. Villeneuve, A. Stolow, P. Corkum, and A. Staudte, Threshold photodissociation dynamics of NO_2 studied by time-resolved cold target recoil ion momentum spectroscopy, The Journal of Chemical Physics **151**, 174301 (2019).
[19] F. Allum, N. Anders, M. Brouard, P. Bucksbaum, M. Burt, B. Downes-Ward, S. Grundmann, J. Harries, Y. Ishimura, H. Iwayama, et al., Multi-channel photodissociation and XUV-induced charge transfer dynamics in strong-field-ionized methyl iodide studied with time-resolved recoil-frame covariance imaging, Faraday Discussions **228**, 571 (2021).
[20] A. J. Howard, M. Britton, Z. L. Streeter, C. Cheng, R. Forbes, J. L. Reynolds, F. Allum, G. A. McCracken, I. Gabalski, R. R. Lucchese, C. W. McCurdy, T. Weinacht, and P. H. Bucksbaum, Filming enhanced ionization in an ultrafast triatomic slingshot (2022).
[21] D. M. Bittner, K. Gope, and D. Strasser, Time-resolved dissociative ionization and double photoionization of CO_2, The Journal of Chemical Physics **153**, 194201 (2020).
[22] T. Endo, S. P. Neville, V. Wanie, S. Beaulieu, C. Qu, J. Deschamps, P. Lassonde, B. E. Schmidt, H. Fujise, M. Fushitani, et al., Capturing roaming molecular fragments in real time, Science **370**, 1072 (2020).
[23] E. Wang, X. Shan, L. Chen, T. Pfeifer, X. Chen, X. Ren, and A. Dorn, Ultrafast proton transfer dynamics on the repulsive potential of the ethanol dication: roaming-mediated isomerization versus Coulomb explosion, The Journal of Physical Chemistry A **124**, 2785 (2020).
[24] N. Ekanayake, T. Severt, M. Nairat, N. P. Weingartz, B. M. Farris, B. Kaderiya, P. Feizollah, B. Jochim, F. Ziaee, K. Borne, et al., H_2 roaming chemistry and the formation of H_3+ from organic molecules in strong laser fields, Nature Communications **9**, 1 (2018).
[25] E. Livshits, I. Luzon, K. Gope, R. Baer, and D. Strasser, Time-resolving the ultrafast H_2 roaming chemistry and H_3+ formation using extreme-ultraviolet pulses, Communications Chemistry **3**, 1 (2020).
[26] K. Gope, E. Livshits, D. M. Bittner, R. Baer, and D. Strasser, Two pathways and an isotope effect in H_3+ formation following double ionization of methanol, Natural Sciences **1**, e10022 (2021).
[27] I. Luzon, E. Livshits, K. Gope, R. Baer, and D. Strasser, Making sense of Coulomb explosion imaging, The Journal of Physical Chemistry Letters **10**, 1361 (2019).
[28] K. Gope, I. Luzon, and D. Strasser, N–NO & NN–O bond cleavage dynamics in two-and three-body Coulomb explosion of the N_2O_2+ dication, Physical Chemistry Chemical Physics **21**, 13730 (2019).
[29] R. Boll, J. M. Schäfer, B. Richard, K. Fehre, G. Kastirke, Z. Jurek, M. S. Schöffler, M. M. Abdullah, N. Anders, T. M. Baumann, et al., X-ray multiphoton-induced Coulomb explosion images complex single molecules, Nature Physics **18**, 423 (2022).
[30] X. Li, A. Rudenko, M. Schöffler, N. Anders, T. M. Baumann, S. Eckart, B. Erk, A. De Fanis, K. Fehre, R. Dörner, et al., Coulomb explosion imaging of small polyatomic molecules with ultrashort x-ray pulses, Physical Review Research **4**, 013029 (2022).
[31] A. Howard, C. Cheng, R. Forbes, G. McCracken, W. Mills, V. Makhija, M. Spanner, T. Weinacht, and P. Bucksbaum, Strong-field ionization of water: Nuclear dynamics revealed by varying the pulse duration, Physical Review A **103**, 043120 (2021).
[32] L. Frasinski, K. Codling, and P. Hatherly, Covariance mapping: A correlation method applied to multiphoton multiple ionization, Science **246**, 1029 (1989).
[33] I. Noda, Generalized two-dimensional correlation method applicable to infrared, raman, and other types of spectroscopy, Applied Spectroscopy **47**, 1329 (1993).
[34] L. J. Frasinski, Covariance mapping techniques, Journal of Physics B: Atomic, Molecular and Optical Physics **49**, 152004 (2016).
[35] J. D. Pickering, K. Amini, M. Brouard, M. Burt, I. J. Bush, L. Christensen, A. Lauer, J. H. Nielsen, C. S. Slater, and H. Stapelfeldt, Communication: Three-fold covariance imaging of laser-induced Coulomb explosions, The Journal of Chemical Physics **144**, 161105 (2016).
[36] C. S. Slater, S. Blake, M. Brouard, A. Lauer, C. Vallance, J. J. John, R. Turchetta, A. Nomerotski, L. Christensen, J. H. Nielsen, et al., Covariance imaging experiments using a pixel-imaging mass-spectrometry camera, Physical

Review A **89**, 011401 (2014).
[37] J. W. Lee, H. Köckert, D. Heathcote, D. Popat, R. T. Chapman, G. Karras, P. Majchrzak, E. Springate, and C. Vallance, Three-dimensional covariance-map imaging of molecular structure and dynamics on the ultrafast timescale, Communications Chemistry **3**, 1 (2020).
[38] L. Frasinski, V. Zhaunerchyk, M. Mucke, R. J. Squibb, M. Siano, J. H. Eland, P. Linusson, P. Vd Meulen, P. Salén, R. Thomas, et al., Dynamics of hollow atom formation in intense x-ray pulses probed by partial covariance mapping, Physical review letters **111**, 073002 (2013).
[39] V. Zhaunerchyk, L. Frasinski, J. H. Eland, and R. Feifel, Theory and simulations of covariance mapping in multiple dimensions for data analysis in high-event-rate experiments, Physical Review A **89**, 053418 (2014).
[40] J. W. McManus, T. Walmsley, K. Nagaya, J. R. Harries, Y. Kumagai, H. Iwayama, M. N. Ashfold, M. Britton, P. H. Bucksbaum, B. Downes-Ward, et al., Disentangling sequential and concerted fragmentations of molecular polycations with covariant native frame analysis, Physical Chemistry Chemical Physics (2022).
[41] L. J. Frasinski, Cumulant mapping as the basis of multidimensional spectrometry, Physical Chemistry Chemical Physics **24**, 20776 (2022).
[42] Either by symmetry or via the use of a moment generation function.
[43] A. T. Eppink and D. H. Parker, Velocity map imaging of ions and electrons using electrostatic lenses: Application in photoelectron and photofragment ion imaging of molecular oxygen, Review of Scientific Instruments **68**, 3477 (1997).
[44] A. Zhao, M. van Beuzekom, B. Bouwens, D. Byelov, I. Chakaberia, C. Cheng, E. Maddox, A. Nomerotski, P. Svihra, J. Visser, et al., Coincidence velocity map imaging using Tpx3Cam, a time stamping optical camera with 1.5 ns timing resolution, Rev. Sci. Instrum. **88**, 113104 (2017).
[45] A. Catanese, B. Kaufman, C. Cheng, E. Jones, M. G. Cohen, and T. Weinacht, Acousto-optic modulator pulse-shaper compression of octave-spanning pulses from a stretched hollow-core fiber, OSA Continuum **4**, 3176 (2021).
[46] M. Nisoli, S. De Silvestri, and O. Svelto, Generation of high energy 10 fs pulses by a new pulse compression technique, Applied Physics Letters **68**, 2793 (1996).
[47] T. Nagy, P. Simon, and L. Veisz, High-energy few-cycle pulses: post-compression techniques, Advances in Physics: X **6**, 1845795 (2021).
[48] T. Nagy, M. Forster, and P. Simon, Flexible hollow fiber for pulse compressors, Applied Optics **47**, 3264 (2008).
[49] C. Cheng, R. Forbes, A. J. Howard, M. Spanner, P. H. Bucksbaum, and T. Weinacht, Momentum-resolved above-threshold ionization of deuterated water, Physical Review A **102**, 052813 (2020).
[50] J. Mikosch and S. Patchkovskii, Coincidence and covariance data acquisition in photoelectron and-ion spectroscopy. i. formal theory, Journal of Modern Optics **60**, 1426 (2013).
[51] J. Mikosch and S. Patchkovskii, Coincidence and covariance data acquisition in photoelectron and-ion spectroscopy. II. analysis and applications, Journal of Modern Optics **60**, 1439 (2013).
[52] C.-M. Tseng, M. Fushitani, A. Matsuda, and A. Hishikawa, Coincidence momentum imaging of four-and three-body Coulomb explosion of formaldehyde in ultrashort intense laser fields, Journal of Electron Spectroscopy and Related Phenomena **228**, 25 (2018).
[53] C. Cheng, Z. L. Streeter, A. J. Howard, M. Spanner, R. R. Lucchese, C. W. McCurdy, T. Weinacht, P. H. Bucksbaum, and R. Forbes, Strong-field ionization of water. II. electronic and nuclear dynamics en route to double ionization, Physical Review A **104**, 023108 (2021).
[54] T. Seideman, M. Y. Ivanov, and P. B. Corkum, Role of electron localization in intense-field molecular ionization, Physical Review Letters **75**, 2819 (1995).
[55] I. Bocharova, R. Karimi, E. F. Penka, J.-P. Brichta, P. Lassonde, X. Fu, J.-C. Kieffer, A. D. Bandrauk, I. Litvinyuk, J. Sanderson, et al., Charge resonance enhanced ionization of CO_2 probed by laser Coulomb explosion imaging, Physical Review Letters **107**, 063201 (2011).
[56] H. Liu, M. Li, X.-G. Xie, C. Wu, Y.-K. Deng, C.-Y. Wu, Q.-H. Gong, and Y.-Q. Liu, Charge resonance enhanced multiple ionization of H_2O molecules in intense laser fields, Chinese Physics Letters **32**, 063301 (2015).
[57] F. Légaré, I. Litvinyuk, P. Dooley, F. Quéré, A. Bandrauk, D. Villeneuve, and P. Corkum, Time-resolved double ionization with few cycle laser pulses, Physical Review Letters **91**, 093002 (2003).
[58] S. Koh, K. Yamazaki, M. Kanno, H. Kono, and K. Yamanouchi, Ionization and dissociation dynamics of H_2O in ultrashort intense near-IR laser fields by the time-dependent adiabatic state method and the time-dependent configuration interaction method, Chemical Physics Letters **742**, 137165 (2020).
[59] J. Rajput, T. Severt, B. Berry, B. Jochim, P. Feizollah, B. Kaderiya, M. Zohrabi, U. Ablikim, F. Ziaee, D. Rolles, et al., Native frames: Disentangling sequential from concerted three-body fragmentation, Physical Review Letters **120**, 103001 (2018).
[60] T. Severt, Z. L. Streeter, W. Iskandar, K. A. Larsen, A. Gatton, D. Trabert, B. Jochim, B. Griffin, E. G. Champenois, M. M. Brister, et al., Step-by-step state-selective tracking of fragmentation dynamics of water dications by momentum imaging, Nature Communications **13**, 1 (2022).